NeuroImage **15,** 273–289 (2002)
doi:10.1006/nimg.2001.0978, available online at http://www.idealibrary.com on IDEAL®

TECHNICAL NOTE

Automated Anatomical Labeling of Activations in SPM Using a Macroscopic Anatomical Parcellation of the MNI MRI Single-Subject Brain

N. Tzourio-Mazoyer, B. Landeau,* D. Papathanassiou, F. Crivello, O. Etard, N. Delcroix, B. Mazoyer,† and M. Joliot[1]

*Groupe d'Imagerie Neurofonctionnelle, UMR 6095 CNRS CEA, Université de Caen, Université de Paris 5; *INSERM U320, Caen; and †Unité IRM, CHU de Caen, and Institut Universitaire de France, Caen, France*

Received April 10, 2001

An anatomical parcellation of the spatially normalized single-subject high-resolution T1 volume provided by the Montreal Neurological Institute (MNI) (D. L. Collins *et al.*, 1998, *Trans. Med. Imag.* 17, 463–468) was performed. The MNI single-subject main sulci were first delineated and further used as landmarks for the 3D definition of 45 anatomical volumes of interest (AVOI) in each hemisphere. This procedure was performed using a dedicated software which allowed a 3D following of the sulci course on the edited brain. Regions of interest were then drawn manually with the same software every 2 mm on the axial slices of the high-resolution MNI single subject. The 90 AVOI were reconstructed and assigned a label. Using this parcellation method, three procedures to perform the automated anatomical labeling of functional studies are proposed: (1) labeling of an extremum defined by a set of coordinates, (2) percentage of voxels belonging to each of the AVOI intersected by a sphere centered by a set of coordinates, and (3) percentage of voxels belonging to each of the AVOI intersected by an activated cluster. An interface with the Statistical Parametric Mapping package (SPM, J. Ashburner and K. J. Friston, 1999, *Hum. Brain Mapp.* 7, 254–266) is provided as a freeware to researchers of the neuroimaging community. We believe that this tool is an improvement for the macroscopical labeling of activated area compared to labeling assessed using the Talairach atlas brain in which deformations are well known. However, this tool does not alleviate the need for more sophisticated labeling strategies based on anatomical or cytoarchitectonic probabilistic maps.

INTRODUCTION

One of the major goals of modern human neuroscience research is to establish the relationships between brain structures and their functions and to reduce the anatomical and functional variability which is considerable between subjects. To reduce the anatomical variability, the first step of group analysis in activation studies consists of applying tools for spatial registration and normalization of brain images taken from different individuals. This can be achieved using, in particular, the procedure implemented in the Statistical Parametric Mapping package (SPM, Friston *et al.*, 1995b; Ashburner and Friston, 1999). In the SPM99 package the target brain for spatial normalization consists in the average of 152 brains (MNI average), supplied by the Montreal Neurological Institute (MNI) (Collins *et al.*, 1994). However, because of the lack of detailed anatomical features on the average anatomical image, functional imaging results are usually overlaid on a high-resolution single-subject T1-weighted MR, termed the MNI single subject in this work. Since this brain is not anatomically labeled, most researchers prefer the use of the Talairach atlas (Talairach and Tournoux, 1988) to report the localization of the activations detected in functional imaging studies, because it offers a detailed anatomical brain description within the stereotaxic space, including Brodmann's areas (BA). However, assigning a set of coordinates to an anatomical label using the paper Talairach atlas is quite inaccurate for several reasons:

[1] To whom correspondence and reprint requests should be addressed at Groupe d'Imagerie Neurofonctionnelle, GIP Cyceron, Boulevard Becquerel, BP 5229, 14074 Caen Cedex, France. Fax: +33 231 470 222. E-mail: joliot@cyceron.fr.

1053-8119/02 $35.00

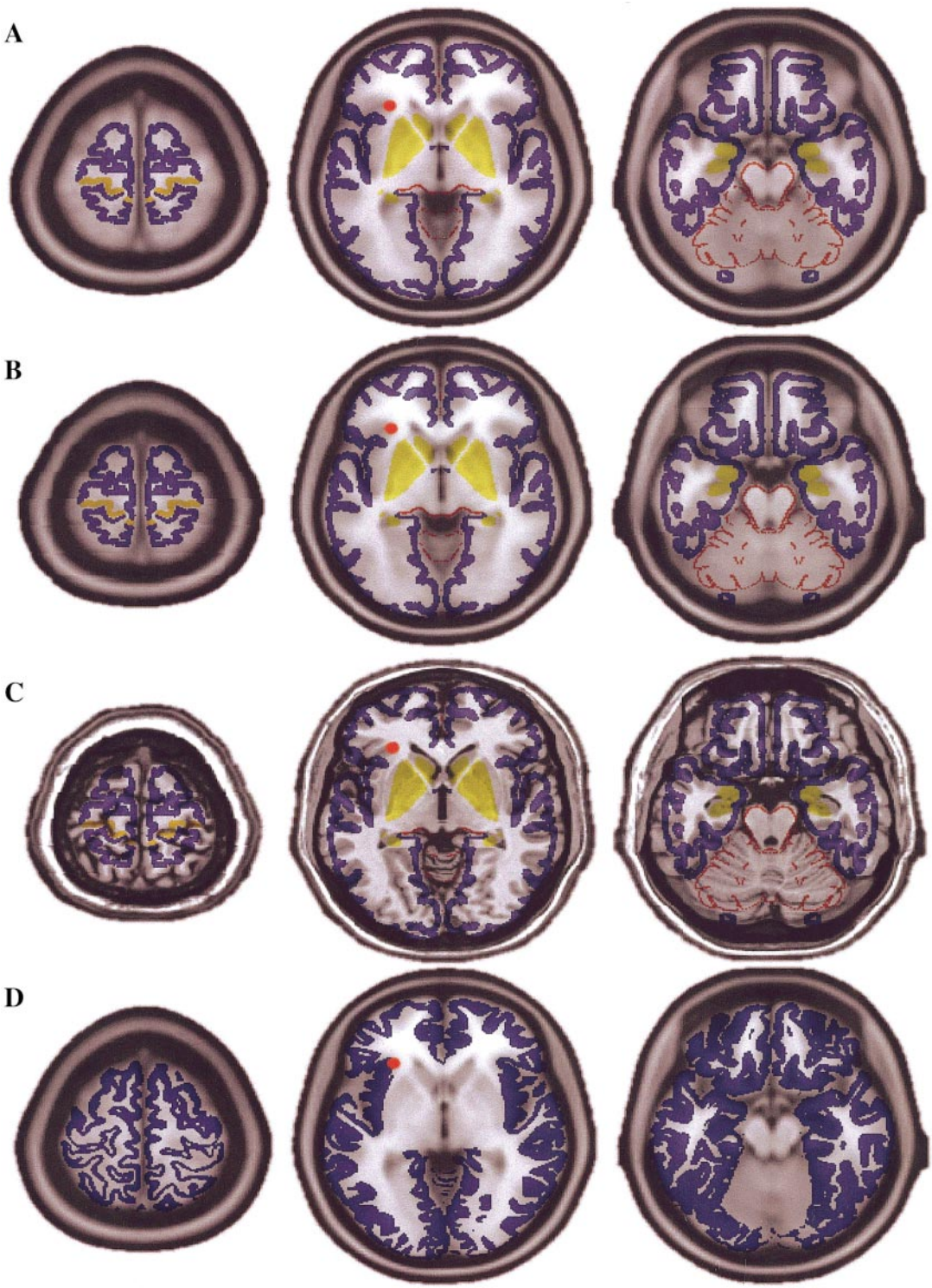

FIG. 1. (A) Overlay of the Talairach atlas on the T1 average of 152 subjects. (B) Overlay of the Talairach atlas on the T1 average of 152 subjects after the nonlinear correction proposed by the MRC Cognition and Brain Sciences Unit (Cambridge, England, http://www.mrc-cbu.cam.ac.uk/Imaging/mnispace.html). (C) Overlay of the Talairach atlas on the T1 single-subject template after the nonlinear correction. (D) Overlay of the cortical gray matter of the T1 single-subject template on the T1 average of 152 subjects. (Cortical strip, blue; Rolando sulcus anterior cortical bank, light orange; subcortical structures, yellow; cerebellum, orange). The Talairach right hemisphere was computer graphically created as the mirror image of the left hemisphere. The red dot indicates a region labeled as Broca's area with reference to Talairach atlas and insula on the MNI single subject.

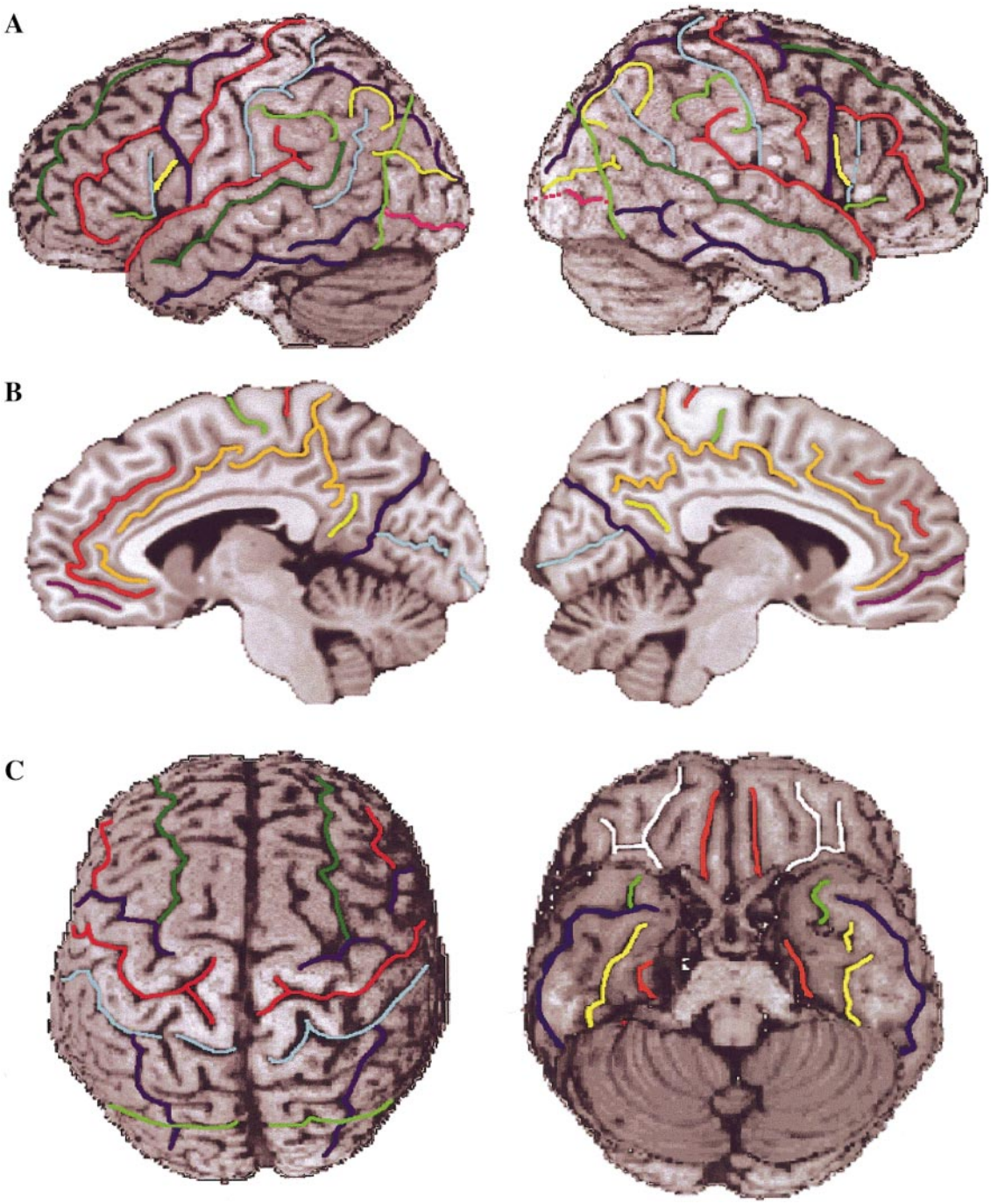

FIG. 2. Sulci definition on the three-dimensional renderings of the T1 MNI single-subject brain: (A) Lateral view; left hemisphere is on the left. From front to back one finds in the superior part of the hemispheres the following sulci: superior frontal (dark green), inferior frontal (red), horizontal ramus of the sylvian fissure (light green), vertical ramus (cyan), diagonal sulcus (yellow, not used for the parcellation), precentral (purple), Rolando (red), postcentral (cyan), intraparietal and intraoccipital (purple), anterior limit of the occipital lobe, corresponding in its inferior part to the anterior occipital sulcus (light green), transverse occipital (yellow), inferior occipital (pink). From top to bottom, in the inferior part of the hemisphere: sylvian fissure (red), superior temporal (dark green), angular (cyan), and inferior temporal (dark blue). (B) Parasagittal medial view, from front to back: paracingulate (red), cingulate (orange), anterior rostral sulcus (purple, not used for the parcellation), paracentral (light green), Rolandic sulcus (red), marginal ramus (orange), subparietal sulcus (yellow), parietooccipital sulcus (blue), and calcarine fissure (cyan). (C) Superior view: the superior frontal (dark green) runs in the same direction and is symmetric in an horizontal plane with the intraoccipital sulcus (purple), rolandic sulcus (red), the precentral (purple) and the postcentral (cyan) run parallel. Inferior view: in the frontal lobe are depicted the orbital (white) and olfactory (red) sulci. In the temporal lobe: rhinal sulcus (light green), inferior temporal (dark blue), occipitotemporal (yellow), and collateral fissure (red). (The dotted lines represents the extended limits used for parcellation.)

the sampling of the Talairach brain is coarse (4 mm), a single hemisphere is labeled, and there are a lot of ambiguities when the point defined by a set of coordinates falls in between different brain areas. To improve this procedure, some authors have proposed an automatic labeling of activations based on the Talairach atlas (Lancaster *et al.,* 2000), to provide a hierarchical classification including BA as the cell type. The principle of this approach is of interest because it offers a reference frame for activation labeling, but the loose relationship existing between BA as defined in the Talairach atlas, and both the functional and the structural anatomy, is a serious drawback. As a matter of fact, there is such a large intersubjects' variability in cytoarchitectonic areas that one cannot consider such labeling as reliable (Rajkowska and Goldman-Rakic, 1995) out of the primary cortices (Rademacher *et al.,* 1993). Moreover a rigorous cytoarchitectonic classification requires the use of automated cytoarchitectonic definition (Schleicher *et al.,* 1999). In addition, even with the help of an automated procedure, the labeling of activation based on the Talairach atlas remains inaccurate since, when researchers refer to this brain atlas after images spatial normalization, the correspondence between the Talairach atlas brain and either the MNI average template (Figs. 1A and 1B) or the MNI single-subject template (Fig. 1C) is not satisfactory. There is, indeed, a larger extent of the MNI single-subject template in the *z* axis, and Talairach's brain shows deformations in its posterior part. As a matter of fact, this brain is a specimen of a 60-year-old female brain that had been kept for years in formol. Thus, one should not be surprised to observe anatomical differences between this *ex vivo* preparation with the *in vivo* MRI of a young male adult. Some authors (MRC Cognition and Brain Sciences Unit, Cambridge, England, http://www.mrc-cbu.cam.ac.uk/Imaging/mnispace.html) have proposed an empirical algorithm to make the correspondence between the coordinates obtained from images normalized with the MNI average template as the target and the Talairach atlas brain (see Fig. 1B). After such correction, because of the intrinsic deformation of the brain labeled in the latter atlas, errors in anatomical labeling are still present that can be of importance in the interpretation of functional imaging studies. For example, a region labeled as Broca's area with reference to Talairach atlas may correspond to the insula on the MNI single-subject template because of both the differences in brain size and the presence of cortical atrophy in the Talairach atlas's brain (see Fig. 1B). As the MNI single-subject template is provided spatially registered and normalized to the MNI average template, the overlay of these two templates is free from any gross anatomical mismatch. This is shown in Fig. 1D, where a segmentation of the gray matter of the MNI single-subject template was overlaid on the MNI average template. Note for example the good match in the upper regions of the brain and in both insula compared to the poor match exhibited with the Talairach atlas (Fig. 1B).

In the present study we propose an automated anatomical labeling of activations detected with PET or fMRI studies, based on an anatomical parcellation of the MNI single-subject brain using a method developed in our laboratory (Tzourio *et al.,* 1997). This work does not aim at solving the question of interindividual anatomical variability which remains from 9 to 18 mm after an affine stereotaxic normalization, depending on the brain regions considered (Thompson *et al.,* 1996). Indeed, the anatomical labeling from a single-subject MRI does not provide the absolute anatomical localization that can only be determined by reference to individual anatomy or approximated by reference to anatomical probabilistic maps. Rather, the purpose of this work was to suppress the confusion existing in the literature regarding the relationship between a set of coordinates and its anatomical label. This is an important issue, since the strength of the stereotaxic normalization methodology is to provide a common system of reference in functional imaging research which at present blurred by the lack of an adapted and convenient tool for the last step in the procedure, namely, reporting on the localization of activations. We will first give an overview of the method and then a detailed description of the anatomical parcellation is provided along with an application routine.

OVERVIEW OF THE METHOD

MNI Single-Subject Images

The MNI single-subject MRI brain template used in the present study comes from the Montreal Neurological Institute database. This brain template was obtained from the MRI acquisition of a young man whose brain was scanned 27 times using a T1-weighted gradient echo sequence (TR/TE/FA = 18 ms/10 ms/30°). Each acquisition was corrected for inhomogeneities (Sled *et al.,* 1998) and spatially normalized (Collins *et al.,* 1994) using a linear nine-parameter transformation. The average of the 27 acquisitions was provided to be used with their MNI web brain simulator (Collins *et al.,* 1998) and with the statistical parametric mapping package (SPM; Friston *et al.,* 1995b; Ashburner and Friston, 1999). In addition, a segmentation in eight classes including gray matter, white matter, cerebrospinal fluid, fat, muscle/skin, skin, skull, and glial matter has been made available. In the SPM package this data set was given the name "single_subj_T1" and was sampled in 8-mm^3 cubic voxels. For the present work we used the high-resolution version (1-mm^3 cubic voxels) after removing nonbrain tissues through the use of a custom-built software program (Quinton *et al.,* 1997).

Sulci Delineation

The sulci course was first tracked using both the three-dimensional hemisphere surface renderings and the slice displays in the three major incidences (axial, sagittal, coronal), a method which allows one to circumvent the anatomical ambiguities present when working on a single incidence. The sulci were then drawn on the 3D rendering of the cortical surfaces (Fig. 2). This was performed after applying a software developed in our laboratory (Voxeline, Diallo *et al.*, 1998) allowing, as others have shown (Frank *et al.*, 1997), 3D tracking and drawing of anatomical landmarks both on the external surface of the hemisphere and on any incidences.

Regions Drawing

Regions of interest (ROI) were drawn manually every 2 mm on axial slices (Figs. 3 and 4) using Voxeline that includes tools for 2D region of interest manual delineation. The sulci landmarks were used as the limits of the ROI on the outer surface of the brain. Starting from the landmark, inner boundaries were traced along the sulci internal course. The ROI internal limit was defined as the 60% isocontour obtained on the PET template of SPM99, although when, due to partial volume effect, some gray matter appeared internally to the isocontours it was included in the ROI.

3D Anatomical Volumes of Interest (AVOI)

Each region was two dimensionally filled using a four-neighbors connectivity algorithm (edges connections), and for each anatomical region a 3D AVOI, including all its 2D pieces, was created. For each AVOI we created both a 1- and a 8-mm^3 sampled volume. As the initial ROI were drawn every 2 mm in the inferior–superior direction, the 1-mm^3 volume was calculated using a nearest neighbor interpolation scheme to create a 2D region on the untraced axial slices. Each AVOI was then given a gray-level code and included in the global templates. We also computed the volume showing only the outline of the anatomical regions.

Automated Anatomical Labeling

We implemented three procedures for the automatic anatomical labeling of the functional activation map: (1) local maxima labeling, (2) extended local maxima labeling, and (3) cluster labeling. Each type of labeling procedure assumes that the functional map has been spatially normalized using the MNI template. In the first step, the functional map is thresholded and then both the local maxima and the clusters are extracted. The three procedures are described bellow and graphically illustrated in Fig. 5.

Local maxima labeling (Fig. 5A) is the simple assignment of the label of the AVOI it belongs to. If the local maxima does not belong to any AVOI, the labels of the three nearest anatomical regions are listed as well as the smallest distance between these AVOI and the local maxima.

In extended local maxima labeling (Fig. 5B), a spherical volume surrounding the local maxima is defined. The radius of this region is chosen by the user (a reference value of 10 mm is used in our laboratory, see Discussion). For each AVOI we compute the number of voxels overlapping this spherical region. The none null numbers are expressed in percentage of overlap to the total number of voxels of the spherical volume and sorted in a descending order. Note that if some parts of the spherical volume fall outside any AVOI, a label "outside" is included in the list.

In cluster labeling (Fig. 5C), we use the same procedure as the extended local maxima labeling, replacing the spherical volume by the functional cluster.

SPM Anatomical Labeling Interface

The three procedures were coded in Matlab in order to be compatible with the SPM result data structure. The procedures are called through different command lines under the Matlab environment. Each procedure prompts the user for the Matlab result file to be analyzed and all the parameters asked in a regular SPM result analysis: contrast, statistical threshold, and minimum cluster size, using the "spm_getSPM" routine of SPM. This routine extracts, for the selected contrast, the clusters and for each cluster the three more significant local maxima (separated by more than 8 mm). In the following step, the user chooses an AVOI template, namely either the 1- or the 8-mm^3 templates. The choice between the two templates is a tradeoff between resolution (better in the 1mm^3) and speed (faster in the 8mm^3). The three labeling methods output are redirected on the "Graphics" window of SPM as a table (see Fig. 6 in the result section for an example) including the local maxima stereotaxic coordinates and its anatomical label. For the cluster labeling, only the most significant local maxima stereotaxic coordinates are listed. For the local maxima labeling, the distance is added to the table and, for the extended local maxima and cluster labeling, the percentage of overlap is shown.

MNI SINGLE-SUBJECT BRAIN PARCELLATION

Sulci Identification

For the purpose of the anatomical parcellation we identified 31 sulci: 18 on the lateral surface of each hemisphere (Table 1, Fig. 2A), plus, in the depth of the cortical mantle, the circular sulcus of the insula and the deep temporal sulcus, 7 on each of the medial interhemispheric surface (Fig. 2B) and 6 on each of the

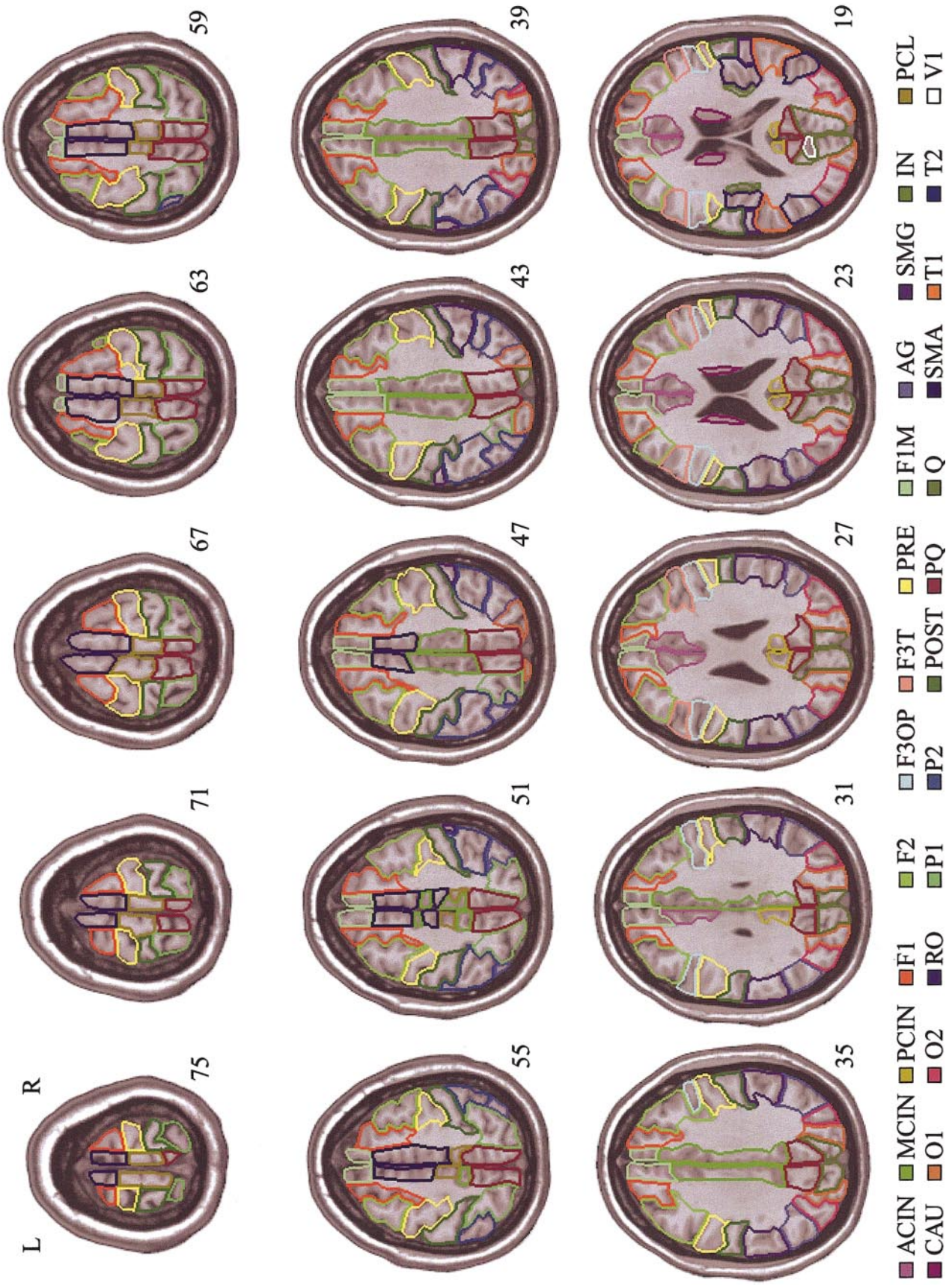

FIG. 3. Regions of interest drawn on axial 1-mm-thick T1 MNI single-subject slices (only one slice every 4 mm is reproduced). Labels correspond to those of Table 2. Values on the lower right of each slice indicate the stereotaxic z coordinate in millimeters (from $z = 75$ to $z = 19$ mm).

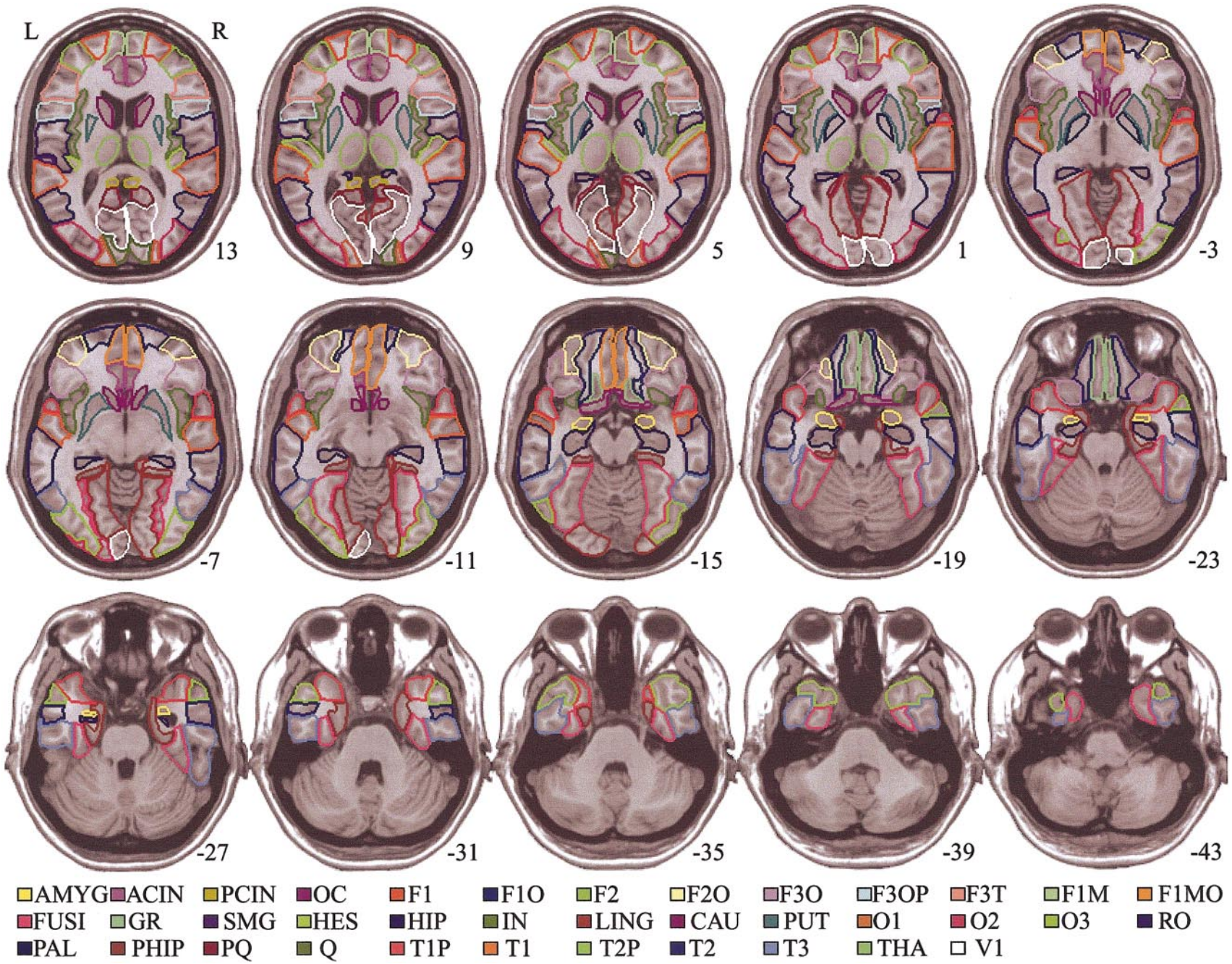

FIG. 4. Regions of interest drawn on axial 1-mm-thick T1 MNI single-subject slices (only one slice every 4 mm is reproduced). Labels correspond to those of Table 2. Values on the lower right of each slice indicate the stereotaxic *z* coordinate in millimeters (from z = 13 to *z* = −43 mm).

inferior brain surface (Fig. 2C). We chose to select constant sulci, primary and secondary sulci in terms of their apparition during fetal life (Chi *et al.*, 1977). We made an exception for the inferior temporal sulcus that develops later in the brain maturation and shows an important variability in terms of its course, number of segments, and types of ending (Ono *et al.*, 1990) because it was identifiable in both hemispheres and allowed the split of the middle and inferior temporal gyri.

In order to document the MNI single-subject brain anatomy with respect to sulcal variability, we show the probability as reported in the Ono statistical brain atlas (Ono *et al.*, 1990) only when a particular anatomical configuration was met (probability $<50\%$). The probabilities are given in percentages, in brackets, L and R referring to the left and right hemisphere, respectively.

Lateral Surface of the Hemispheres

The central region: Rolandic, postcentral, and precentral sulci. To identify the Rolandic sulcus (also termed the central sulcus) we used four criteria: (1) on upper axial slices, the Rolandic sulcus is characterized by a typical notch (Rumeau *et al.*, 1994; Sastre-Janer *et al.*, 1998) and never connects with any of surrounding sulci that run in a different direction such as the superior frontal sulcus or the intraparietal sulcus (Kido *et al.*, 1980); (2) it is always located between two parallel sulci, namely the precentral and the postcentral sulci (Fig. 2A); (3) on the paramedial sagittal slices, on the vertex, the Rolandic sulcus forms a notch just in front of the end of the ascending part of the marginal sulcus (Steinmetz *et al.*, 1990; Berger *et al.*, 1990; Sobel *et al.*, 1993); and (4) on lateral sagittal slices, the Rolandic sulcus is the third sulcus encountered when starting from the ascending branch of the sylvian fissure and moving caudally. Identification of the Rolandic sulcus in both hemispheres was easy: it showed no interruption but we noted two particularities. On the vertex, the Rolandic sulci ended with a "y" shape (Fig. 2C, left) (L 0%, R 28%) and the left Rolandic sulcus showed an anastomosis with the precentral sulcus at the hemisphere surface (Fig. 2A, left) (0%). Once the Rolandic sulcus was identified, it was easy to locate the precentral and postcentral sulci that both run parallel, rostrally and caudally, respectively. In the left hemisphere, the precentral sulcus showed an uninterrupted course to the vertex after its anastomosis in its lower part with the Rolandic sulcus. In the right hemisphere, it was constituted of two segments, making a "pli de passage" above its meeting point with the inferior frontal sulcus (Fig. 2A, right). The postcentral sulci were in two segments in both hemispheres and met the sylvian fissure on both sides.

The frontal lobe: Superior and inferior frontal sulci and ascending and horizontal Sylvian rami. Within the frontal lobe, the superior frontal sulci started on the vertex by an anastomosis perpendicular to the precentral sulcus and showed no interruption in their course (L 32%, Fig. 2C, left). The middle frontal sulcus was clearly seen on lateral sagittal slices, describing a curve from its anastomosis with the lower third of the precentral sulcus toward the anterior part of the sylvian fissure that it reached neither in the right nor in the left hemisphere (Fig. 2A). The horizontal ramus of the sylvian fissure was clearly seen in both hemispheres, as well as the ascending ramus, intercepted by the diagonal sulcus on both sides (Fig. 2A).

The temporal lobe: Sylvian fissure and superior and middle temporal sulci. The sylvian fissure was easy to identify, moving across the brain and following an uninterrupted anteroposterior course. Its start constituted the limit between the temporal pole and the frontal lobe, and it ended caudally by a bifurcation into two sulci: one ascending and one descending. The terminal ascending segment of the sylvian fissure was clearly seen on MNI single-subject cortical surfaces in both hemispheres (Fig. 2A).

The left superior temporal sulcus (t1) started at a small distance from the pole, showing a vertical ending parallel to the sylvian fissure. In this hemisphere the angular sulcus, representing the center of the angular gyrus, was the posterior parallel of the posterior ending of t1. In the right hemisphere t1 showed a horizontal course, and the angular sulcus was anterior to t1 posterior ending.

The middle temporal sulci started at the temporal pole, with only one interruption in each hemisphere (R 8%, L 0%). On the left, an accessory sulcus was present in its midpart, connecting it to a lower segment of t1. In the right hemisphere it ended caudally by its union with the anterior occipital sulcus (R 4%), while in the left side it merged with the inferior occipital sulcus (L 0%).

The parietal lobe and occipital lobe. The intraparietal sulcus was identified in both hemispheres as a very deep sulcus starting by a long connection within the midpoint of the internal–external course of the postcentral sulcus on the superior view of the brain (Fig. 2C, left), showing an anteroposterior course in the parietal lobe and joining the occipital lobe to become the intraoccipital sulcus. It was divided in two segments on both sides.

The inferior occipital sulcus (Dejerine, 1980) was in the continuation of the posterior segment of the middle temporal sulcus and showed no interruption until its ending at the occipital pole in the left hemisphere. On the right, the inferior occipital sulcus was reduced to a very small segment, symmetrical to the left.

The anterior occipital sulcus was identified in both hemispheres as the sulcus starting from the inferior border of the lateral surface of the hemisphere, nearby

the preoccipital notch (also called Meynert notch), at the junction between the occipital and inferior temporal gyri. It followed a short vertical course, forming the anterior limit of the occipital lobe in its inferior part.

Internal Surface of the Hemispheres

Frontal lobe: Cingulate, paracingulate, and paracentral sulci. The cingulate sulci were present in both hemispheres, showing two interruptions on both sides. The anterior origin of the cingulate sulcus showed no connection with the anterior rostral sulcus (Fig. 2B) in either hemisphere. In the left hemisphere there was a continuous paracingulate or intralimbic sulcus duplicating the cingulate sulcus upward (Paus *et al.*, 1996). In the right hemisphere the paracingulate sulcus was limited to two small segments. The marginal ramus of the cingulate sulcus was also identified to serve as the posterior limit of the paracentral gyrus in both hemispheres.

The paracentral sulcus was identified as the sulcus anterior to the Rolandic notch on the internal surface of each hemisphere. It started nearby the posterior part of the cingulate sulcus and followed a posteroanterior course in direction of the vertex. In the right hemisphere it was a side branch of the cingulate sulcus (24%), while in the left hemisphere it was connected to the lateral surface (12%).

In both hemispheres subparietal sulci were located in a vertical axis, posterior to the corpus callosum posterior side, as a small free sulcus on both sides (R 4%, L 8%).

Occipital lobe: Parietooccipital sulcus and calcarine fissure. The parietooccipital sulcus, a constant and deep primary sulcus, showed a caudorostral and dorsoventral course that was clearly seen on both internal hemispheric surfaces (Fig. 2B). The calcarine fissure started at the occipital pole in the right hemisphere and followed an uninterrupted course in a caudorostral and ventrocaudal direction toward its junction with the parietooccipital sulcus, at its inferior third. In the left hemisphere its course started at the occipital pole, showed an interruption, and then had a continuous course toward the inferior third of the parietooccipital sulcus.

Inferior Surface of the Hemisphere

Frontal lobe: The third frontal sulcus, the fourth frontal sulcus, or olfactory sulcus. In the orbital part of the frontal lobe we identified the third frontal sulcus (or orbital sulcus), that described a "y" trajectory in both hemispheres. This sulcus allowed us to limit, internally, the orbital parts of the inferior and middle frontal gyri, and externally, the orbital part of the superior frontal gyrus (Dejerine, 1980). We were also able to draw the olfactory sulcus that represents the outer limit of the gyrus rectus and the internal limit of the orbital part of the superior frontal gyrus and describes a deep line parallel to the interhemispheric plane (Fig. 2C).

Temporal lobe: Collateral fissure, rhinal sulcus, and occipitotemporal sulcus. The collateral fissure was identified in both hemispheres on sagittal slices as a deep sulcus showing an anteroposterior uninterrupted course. It showed a single posterior end and no lateral side branch in the right hemisphere (24%) as well as in the left hemisphere (36%). It gave the parahippocampal ramus bilaterally as a side branch of the main trunk, a frequent pattern that marks the posterolateral end of the hippocampus.

The occipitotemporal sulcus, using the denomination of Ono, presented three segments in the left hemisphere, with a long posterior end in the occipital pole. In the right hemisphere it was made of two segments and ended, as in the left hemisphere, in the occipital pole.

The anterior part of the rhinal sulcus was short in both hemispheres and did not show any connection either with the collateral fissure or with the occipitotemporal sulcus (Fig. 2C, right). One should note in the left hemisphere an anastomosis with the anterior ending of the middle temporal sulcus, a configuration not described by Ono *et al.* (1990).

Regions Definition

We used the sulci to delineate 45 AVOI in each hemisphere, as listed in Table 2, although we had to add arbitrary limits in some cases. The vertical plane passing by the anterior commissure (VAC) was used as the posterior limit of the temporal pole, for the superior and middle temporal gyri. A plane located 20 mm forward and parallel to VAC was used for the anterior limit of SMA. A horizontal plane, going through the point where the sylvian fissure starts its verticalization and gives a side branch, was used as a limit between the superior temporal gyrus (ventrally) and the supramarginalis gyrus (dorsally). The ascending and horizontal Sylvian branches were prolonged in order to delineate the opercularis, triangularis, and orbitalis parts of the inferior frontal gyrus. To define the limit between the occipital and parietal lobes we drew a line from the top of the parietooccipital sulcus descending toward the preoccipital notch. Along its trajectory, this line met the anterior occipital sulcus in both hemispheres, providing a good delineation between the occipital and temporal lobe in the inferior third of the hemispheres.

Central Region

Precentral gyrus and postcentral gyrus. The precentral gyrus was defined as the region limited ros-

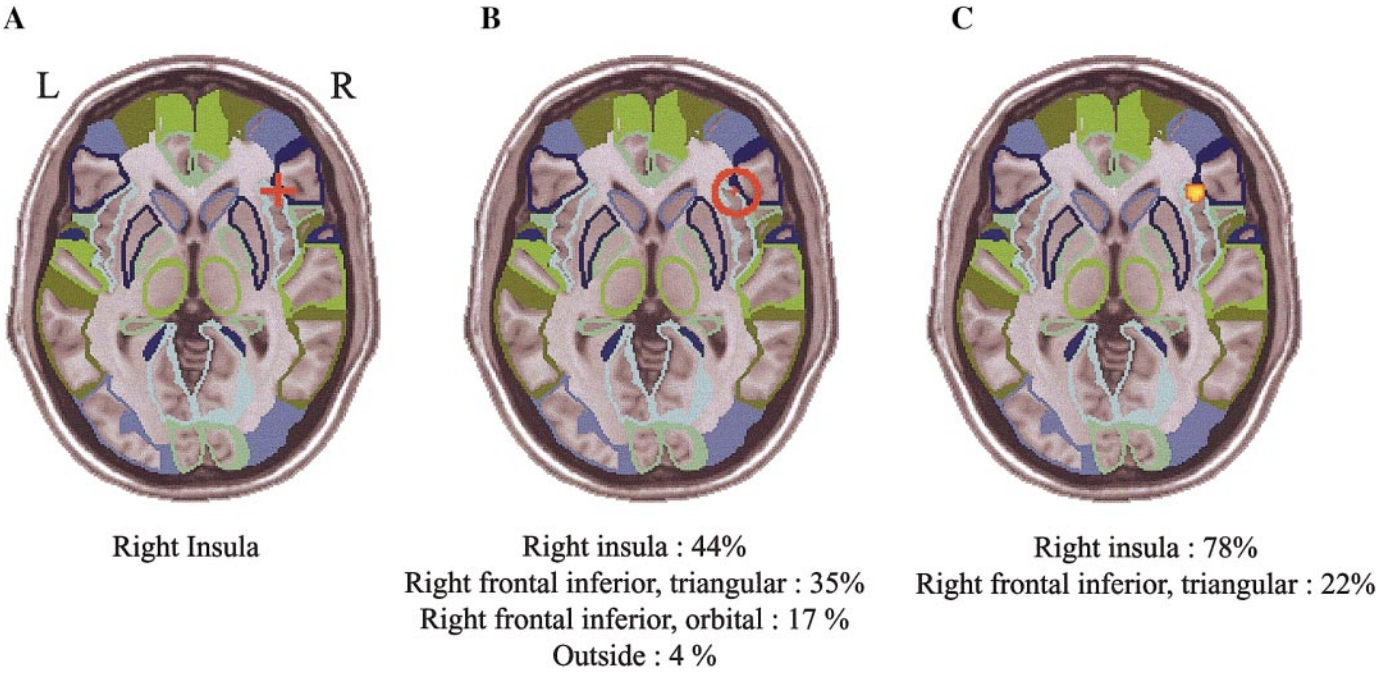

FIG. 5. Illustration of the use of the parcellation and the labeling procedures of functional activation local maxima and cluster. The outline of the parcellation was overlaid on the MNI single-subject $z = 0$ mm axial slice. (A) Local maxima labeling: the red cross indicates the location of the local maximum (stereotaxic coordinates 40, 26, 0 mm). (B) Extended local maxima labeling: percentage of overlap between a 10-mm sphere radius centered on the local maximum and the AVOI parcellation. (C) Cluster labeling: percentage of overlap between the activation cluster and the AVOI parcellation.

trally by the precentral sulcus and caudally by the Rolandic sulcus, while the postcentral region ran caudally parallel to it, limited rostrally by the Rolandic sulcus and caudally by the postcentral sulcus.

Rolandic operculum. The limits of this region were based on the definition given by Dejerine (1980). It was constituted by the region lateral to the posterior convolutions of the insula for its internal part and by the union of the precentral and postcentral gyri after the Rolandic sulcus ends for its lateral part. Neither the opercular part of the inferior frontal gyrus nor the posterior part of the parietal operculum belonged to this region. These are parts of the pars opercularis of the inferior frontal gyrus and of the supramarginalis gyrus, respectively.

Frontal Lobe Lateral Cortex

The superior, middle, and inferior frontal gyri. The superior frontal gyrus was limited by the superior frontal sulcus externally and did not include the cortical gray matter of the internal surface of the brain that belonged to the medial superior frontal region. The middle frontal gyrus was limited caudally by the precentral sulcus, ventrally by the middle frontal sulcus, and dorsally and internally by the superior frontal sulcus. The inferior frontal gyrus was limited by the inferior frontal sulcus dorsally and rostrally and by the precentral sulcus caudally. We subdivided this region in three parts: the pars opercularis, the pars triangularis, and the pars orbitalis. The rostral limit of the pars opercularis was the ascending ramus of Sylvius (the diagonal sulcus although easy to recognize in both hemispheres was not taken into account as a limit) and its caudal limit was the precentral sulcus. The pars triangularis was located in between the inferior frontal sulcus, the horizontal ramus of Sylvius, and the ascending ramus of Sylvius. The pars orbitalis located ventrally to the horizontal Sylvian ramus.

The medial surface of the frontal lobe: Superior frontal gyrus medial part, supplementary motor area, and paracentral lobule. The region of the medial part of the superior frontal gyrus included the gray matter belonging to the internal surface of the hemisphere anterior and superior to the cingulate gyrus from which it was segregated thanks to the paracingulate and cingulate sulci.

The SMA region included the functional definition of SMA and pre-SMA. Its posterior limit was the paracentral sulcus, its inferior limit was the cingulate sulcus, and we choose to use the Talairach atlas anterior limit: 20 mm ahead of the VAC plane. This was done with reference to functional imaging studies that showed that it corresponded to the anterior limit of pre-SMA (for a review see Petit *et al.*, 1998).

A

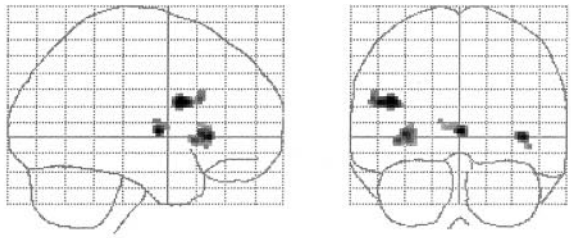

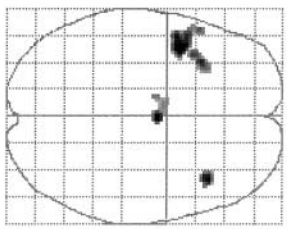

Statistics: *volume summary (p values corrected for entire volume)*

cluster level			voxel level				x,y,z {mm}		
$p_{corrected}$	k_E	$p_{uncorrected}$	$p_{corrected}$	T	(Z)	$p_{uncorrected}$			
0.000	131	0.000	0.046	8.67	(5.21)	0.000	-42	8	22
			0.118	7.87	(4.97)	0.000	-50	6	22
0.000	39	0.000	0.078	8.22	(5.07)	0.000	2	-6	4
0.000	32	0.000	0.113	7.91	(4.98)	0.000	40	26	0
0.000	80	0.000	0.187	7.48	(4.84)	0.000	-34	22	2

B **Labels:** *volume summary (labels for entire volume)*

x,y,z mm	label	mm dist				
-42 8 22	Frontal_Inf_Oper_L	0.00				
-50 6 22	Precentral_L	0.00				
2 -6 4	Thalamus_R	2.83	Thalamus_L	5.66	Caudate_R	11.66
40 26 0	Insula_R	0.00				
-34 22 2	Insula_L	0.00				

C **Labels:** *volume summary (labels and percentages for the entire volume)*

Local Maximum Radius : 10.0mm

x,y,z mm	label	%
-42 8 22	Frontal_Inf_Oper_L	54.37
	Precentral_L	18.64
	Frontal_Inf_Tri_L	12.04
	OUTSIDE	7.57
	Rolandic_Oper_L	6.41
	Insula_L	0.97
-50 6 22	Precentral_L	46.41
	Frontal_Inf_Oper_L	43.88
	Rolandic_Oper_L	5.63
	Frontal_Inf_Tri_L	3.30
	Postcentral_L	0.58
	OUTSIDE	0.19
2 -6 4	OUTSIDE	68.54
	Thalamus_R	19.81
	Thalamus_L	11.65
40 26 0	Insula_R	43.88
	Frontal_Inf_Tri_R	34.37
	Frontal_Inf_Orb_R	17.28
	OUTSIDE	4.08
	Frontal_Inf_Oper_R	0.39
-34 22 2	Insula_L	61.75
	Frontal_Inf_Tri_L	26.60
	OUTSIDE	6.21
	Frontal_Inf_Orb_L	5.44

D **Labels :** *volume summary (labels and percentages per cluster)*

x,y,z mm	label	%
-42 8 22	Frontal_Inf_Oper_L	64.89
	Frontal_Inf_Tri_L	19.85
	Precentral_L	14.50
	OUTSIDE	0.76
2 -6 4	OUTSIDE	97.44
	Thalamus_L	2.56
40 26 0	Insula_R	78.12
	Frontal_Inf_Tri_R	21.88
-34 22 2	Insula_L	100.00

FIG. 6. Illustration of the automated anatomical labeling SPM interface. (A) Maximum intensity projection and corresponding result table as provided by the SPM result section. (B) Output of the local maxima labeling. (C) Output of the extended local maxima labeling, the sphere radius was set at 10 mm. (D) Output of the cluster labeling procedure.

TABLE 1

List of Sulci Defined in Each Hemisphere

Anatomical description
Central region
Precentral
Rolandic
Postcentral
Frontal lobe
Lateral surface
Superior frontal
Middle frontal
Inferior frontal
Ascending ramus of the sylvian fissure
Horizontal ramus of the sylvian fissure
Medial surface
Cingulate
Paracingulate
Marginal ramus
Paracentral
Inferior surface
Third frontal or orbital
Fourth frontal or olfactory
Insular lobe
Circular sulcus of the insula
Temporal lobe
Lateral surface
Sylvian fissure
Superior temporal
Inferior temporal
Deep temporal
Inferior surface
Rhinal
Collateral fissure
Parahippocampal ramus of the collateral fissure
Occipitotemporal
Parietal lobe
Lateral surface
Intraparietal
Angular
Medial surface
Parietooccipital
Subparietal
Occipital lobe
Lateral surface
Anterior occipital
Intraoccipital
Inferior occipital
Medial surface
Calcarine fissure

The caudal limit of the paracentral region was the marginal sulcus, its ventral border was constituted by the cingulate sulcus, and the paracentral sulcus formed its rostral end. In the left hemisphere this sulcus reached the vertex, but in the right side it ended at distance from it and we drew a line that followed the sulcus direction and joined the vertex to complete this rostral limit.

The orbital part of the frontal lobe. In each hemisphere six regions were defined inferior to the AC–PC plane encompassing the orbital parts of the superior, middle, and inferior frontal gyri. Within the internal

TABLE 2

List of the Anatomical Regions of Interest Defined in Each Hemisphere and Their Label

Anatomical description	Label
Central region	
Precentral gyrus	PRE
Postcentral gyrus	POST
Rolandic operculum	RO
Frontal lobe	
Lateral surface	
Superior frontal gyrus, dorsolateral	F1
Middle frontal gyrus	F2
Inferior frontal gyrus, opercular part	F3OP
Inferior frontal gyrus, triangular part	F3T
Medial surface	
Superior frontal gyrus, medial	F1M
Supplementary motor area	SMA
Paracentral lobule	PCL
Orbital surface	
Superior frontal gyrus, orbital part	F1O
Superior frontal gyrus, medial orbital	F1MO
Middle frontal gyrus, orbital part	F2O
Inferior frontal gyrus, orbital part	F3O
Gyrus rectus	GR
Olfactory cortex	OC
Temporal lobe	
Lateral surface	
Superior temporal gyrus	T1
Heschl gyrus	HES
Middle temporal gyrus	T2
Inferior temporal gyrus	T3
Parietal lobe	
Lateral surface	
Superior parietal gyrus	P1
Inferior parietal, but supramarginal and angular gyri	P2
Angular gyrus	AG
Supramarginal gyrus	SMG
Medial surface	
Precuneus	PQ
Occipital lobe	
Lateral surface	
Superior occipital gyrus	O1
Middle occipital gyrus	O2
Inferior occipital gyrus	O3
Medial and inferior surfaces	
Cuneus	Q
Calcarine fissure and surrounding cortex	V1
Lingual gyrus	LING
Fusiform gyrus	FUSI
Limbic lobe	
Temporal pole: superior temporal gyrus	T1P
Temporal pole: middle temporal gyrus	T2P
Anterior cingulate and paracingulate gyri	ACIN
Median cingulate and paracingulate gyri	MCIN
Posterior cingulate gyrus	PCIN
Hippocampus	HIP
Parahippocampal gyrus	PHIP
Insula	IN
Sub cortical gray nuclei	
Amygdala	AMYG
Caudate nucleus	CAU
Lenticular nucleus, putamen	PUT
Lenticular nucleus, pallidum	PAL
Thalamus	THA

face of the superior frontal gyrus orbital, we isolated the medial wall corresponding to the gyrus rectus. It is noteworthy that, the fourth frontal sulcus or olfactory sulcus gives a clear demarcation between the gyrus rectus and the orbital part of the superior frontal gyrus on the inferior surface of the orbital frontal cortex. The third frontal sulcus allowed us to segregate, in the same manner, the middle and inferior frontal gyri orbital parts (Dejerine, 1980). Although it represents a small region, we isolated the olfactory cortices as defined by Dejerine and included in this region the olfactory tubercle, lying in the caudal side of the gyrus rectus within the two branches of the fourth frontal sulcus, and the Broca's olfactory cortex located under the corpus callosum genu.

Temporal Lobe

Planimetry. The planum temporale surfaces defined using the knife cut method of Kulynych *et al.* (1993) were found to be 604 mm^2 on the left side and 797 mm^2 on the right side, a configuration noted very seldom. For this reason we did not delineate the planum temporale, a region showing very high interindividual variability (Westbury *et al.*, 1999) and for which this brain could not be considered as a reference.

Lateral cortex. The superior temporal gyrus was limited dorsally by the sylvian fissure and an horizontal plane starting from its bifurcation, ventrally and caudally by the superior temporal sulcus. We isolated the Heschl or temporal transverse gyrus within the superior temporal gyrus using its configuration in the three incidences and following the criteria used by Penhune *et al.* (1996). The sulcal limits were the deep temporal sulcus caudally and the posterior part of the circular sulcus of the insula rostrally. The middle temporal gyrus was limited dorsally by the superior temporal sulcus, ventrally by the inferior temporal sulcus, and caudally by the anterior occipital sulcus. The temporal pole parts of the superior and middle temporal gyri were isolated as regions anterior to the VAC plane (see limbic lobe).

The inferior temporal gyrus was limited dorsally by the inferior temporal sulcus, internally and ventrally by the occipitotemporal sulcus, and caudally by the anterior occipital sulcus and the preoccipital notch.

Parietal Lobe

Lateral surface: The superior parietal and the inferior parietal lobules including supramarginal and angular gyri. The limits of the superior parietal gyrus were rostrally the postcentral sulcus, externally the intraparietal sulcus, internally the precuneus, and caudally the occipitoparietal line. Within the inferior parietal lobule, we delineated the superior limits of the supramarginal and angular gyri lying around the sylvian fissure ascending branch and the angular sulcus, respectively. The inferior parietal cortex that did not belong to these regions constituted the third region of the inferior parietal lobule. It was located above the supramarginalis gyrus and in between the supramarginal and angular gyri.

Medial surface: The precuneus. The precuneus, on the internal surface of each hemisphere, was limited caudally by the parietooccipital sulcus, rostrally and dorsally by the marginal sulcus, and ventrally by the subparietal sulcus.

Occipital Lobe

Lateral surface: The superior, middle, and inferior occipital gyri. The superior occipital gyrus was delineated using the intraoccipital sulcus as its external border, its internal border being the medial surface gray matter of the cuneus. The middle occipital gyrus was limited internally and dorsally by the intraoccipital sulcus and ventrally by the inferior occipital sulcus. The inferior occipital gyrus was located between the intraoccipital sulcus dorsally and internally, the anterior occipital sulcus rostrally, and the inferior or lateral occipital sulcus ventrally.

Medial surface: The cuneus, calcarine fissure, fusiform, and lingual gyri. The cuneus was defined as the upper part of the medial wall of the occipital lobe, limited rostrally by the parietooccipital sulcus and ventrally by the calcarine fissure. The cortex surrounding the calcarine fissure and its branches constituted the region of the primary visual area.

The lingual gyrus was limited dorsally by the calcarine sulcus, externally and ventrally by the collateral fissure, rostrally by the parietooccipital sulcus, and the parahippocampal ramus of the collateral fissure.

The fusiform gyrus lateral border was the occipitotemporal sulcus, the collateral fissure limiting it internally and ventrally.

The Limbic Lobe

The cingulate regions: Anterior, median, and posterior part of the cingulate gyrus. For the purpose of the cingulate region definition, we drew a limit starting with the paracingulate sulcus on the left and the cingulate on the right and following first the paracingulate sulcus and then, after the two sulci stopped their parallel course, the cingulate sulcus. The caudal limit of the cingulum was set by the subparietal sulcus.

We split the cingulate cortex into anterior, median, and posterior regions using its intersection with the corpus callosum. The anterior cingulate was limited by the paracingulate sulcus rostrally, the white matter of the corpus callosum caudally (Fig. 3 third row, light purple region). The median cingulate region was a continuous region limited dorsally and rostrally by the paracingulate sulcus, caudally by the subparietal sul-

cus, and ventrally by the corpus callosum (Fig. 3, third slice of the second row, green region on the medial surface of the hemispheres). The median cingulate region started 32 mm above the AC–PC plane in the right hemisphere and 34 mm above AC–PC in the left. The posterior cingulate region was limited by the corpus callosum rostrally and the subparietal sulcus caudally (Fig. 3, third row).

The temporal pole. We defined the temporal pole as the region lying forward to VAC that consisted of two regions: the anterior parts of both superior and middle temporal gyri based on the anterior ending of the superior temporal sulcus. The cortex lying between the pole itself and the amygdala, the temporal operculum, was included in the definition of the superior temporal gyrus pole (Mai *et al.*, 1997; Insausti *et al.*, 1998).

The hippocampal and parahippocampal regions. The hippocampal region was defined on the sagittal views as the gray matter espousing the ventricles horns and included the dentate gyrus, the uncus, and the hippocampus proper. It was limited caudally by the parahippocampal ramus of the collateral fissure.

The parahippocampal region consisted of the parahippocampal gyrus and parahippocampal uncus (Talairach and Tournoux, 1988) and included both the entorhinal and the perirhinal cortices. We used for its caudal limit the parietooccipital sulcus, and for its the ventral limit the collateral sulcus. To define its rostral limit we used the criteria of Inausti *et al.* (1998), namely the point where the limen of the insula appears on coronal sections, i.e., a continuous strip of white matter connecting the frontal and temporal lobes. The limit between the hippocampus and parahippocampal gyri in the rostrocaudal and dorsoventral directions was the retrolimbic plicature, giving the limit between the hippocampus and the subiculum.

The Insula and Subcortical Gray Nuclei

The region of the insula was limited externally by the circular sulcus of the insula and included the gray matter internal to this sulcus. The caudate nucleus, the thalamus, and the lenticular nucleus were drawn in each hemisphere using gray matter limits with the surrounding white matter on axial slices. The lenticular nucleus was divided into pallidum and putamen. The amygdala, located rostrally to the hippocampus and caudally to the uncus of the parahippocampal gyrus, was identified using both sagittal and coronal views.

Application to Functional Activation Labeling

The practical use of our labeling method will be illustrated using one of our fMRI experiments (Fig. 6). In this multisubject study of a language-related task, the functional data were normalized using the MNI 152 subjects template. The functional statistical map was thresholded to $P = 0.00001$ (uncorrected for multiple comparison, excluding cluster of less than 30 voxels). In this protocol four clusters and five local maxima were identified, as shown on the maximum intensity projection and the regular SPM table result (Fig. 6A).

With the local maxima approach (Fig. 6B), four of these maxima turned out to be unambiguously labeled. One (stereotaxic coordinates in mm, 2, −6, 4) was localized outside the parcellation, and the three nearest AVOI were thus listed: the right thalamus was found at 2.8 mm, the left thalamus at 5.7 mm, and the right caudate nucleus at 11.7 mm.

The extended local maxima approach (Fig. 6C) was performed with a 10-mm sphere radius. For example, the first local maxima (stereotaxic coordinates −42, 8, 22) was localized mainly in the opercular part of the left inferior gyrus (54%), while the other AVOIs were at less than 20%. The second local maxima (stereotaxic coordinates − 50, 6, 22) was labeled at 46% in the left precentral gyrus and at 43% in opercular part of the left inferior frontal gyrus. These close percentages indicate that this local maxima was in the depth of the precentral sulcus, making it difficult to decide which bank it lied on.

The cluster approach is illustrated in Fig. 6D. The first cluster was mainly labeled as opercular part of the left inferior frontal gyrus (64%) with an extension in the two nearby regions, rostrally in the triangular part (20%) and caudally in the precentral gyrus (14%). The small second cluster was 97% outside the parcellation and only 3% inside the left thalamus.

DISCUSSION

Anatomical Issues

As our labeling scheme relies on the organization of a single brain, we will first discuss the characteristics of the MNI single-subject brain high-resolution template.

MNI single-subject brain. This work uncovered that the MNI single-subject brain showed an absence of leftward anatomical lateralization of the planum temporale that makes it out of the range of standard anatomy. Indeed, the vast majority of right-handers and more than half of left-handers show a leftward asymmetry of this structure (Shapleske *et al.*, 1999). The present brain template was taken from a male subject, known to have larger left planum temporale than females. As matter of fact, the MNI brain template left planum temporale surface was within the range of values described by others using the same method (Kulynych *et al.*, 1994). However, rightward asymmetry of planum temporale, such as the one observed in this brain template, was found in only 10% of the subjects described in this former work. In addition

one should note that several sulcal patterns we described have a low probability with reference to Ono's atlas of the sulci, for example, the ending on the vertex of the Rolandic sulci or the presence of an anastomosis of the precentral sulcus with the Rolandic sulcus in the left hemisphere. It questions the use of a single subject as the reference pattern for anatomical localization in functional imaging studies. However, the purpose of this work was to give a standard reference frame for anatomical labeling of activation, being aware of the importance of interindividual variability, and the quest for a "standard brain" in terms of anatomical pattern would be hazardous. Actually, reference to statistical maps for anatomical labeling in the stereotaxic space is the most accurate solution, although these have not been freely available to researchers until recently (Paus *et al.*, 1996; Penhune *et al.*, 1996; Westbury *et al.*, 1999; Chiavaras and Petrides, 2000).We believe that the detailed description of landmarks used to define sulci using a high-resolution MRI in the present study may be of general interest to the neuroimaging community, as they may serve other investigations to parcellate another template.

AVOI definition. In order to delineate the 3D anatomical volumes of interest we chose to extend the internal limit of the regions beyond the gray matter layer because of the anatomical variability and because of the general lower resolution of functional studies compared to anatomical MRI. Regarding the variability, the definition of regions following strictly the gray matter of this particular brain would have led one to built an atlas parcellation with some of the drawbacks of the Talairach atlas. In such an atlas, because of anatomical gyral variability not accounted for by the normalization, it occurs that some activated regions are localized in the white matter. This drawback is largely avoided with the region definition used in our approach.

Cerebellar AVOIs, based on the cerebellum parcellation proposed by Schmahmann *et al.* (1999), were also included in our computerized parcellation.

Comparison with other parcellations. The present parcellation included the whole brain gray matter and is consistent with others that used sulci as landmarks for regions delineation (Rademacher *et al.*, 1992; Caviness *et al.*, 1996). A main difference concerns the regions where we did not make any subdivision using arbitrary limits as others did for the lateral and inferior temporal cortices (Rademacher *et al.*, 1992; Caviness *et al.*, 1996; Kim *et al.*, 2000). In the temporal lobe, we did not isolate the planum temporale region because of its very large interindividual variability (Westbury *et al.*, 1999). Indeed, the authors of this probabilistic study of the planum temporale limits demonstrated no single voxel being labeled with a probability >65%, which renders the labeling of this region based on a one subject brain inaccurate and misleading. In contrast, we isolated the gyrus of Heschl that had a good overlap on probabilistic maps (Penhune *et al.*, 1996).

Our selected parcellation for the frontal lobe was close to the one proposed by Crespo-Facorro *et al.* (1999), except for the parcellation of the cingulate gyrus. We segregated it in three regions, anterior, middle, and posterior cingulate, while these authors made a large anterior cingulate region including the anterior half of the middle cingulate region of the present study. We chose to isolate the caudal part of the posterior cingulate, namely the retrosplenial cortex, since converging results from functional studies attributed to this region a role in both episodic memory and emotion (Buckner *et al.*, 1996; Maddock, 1999). Similarly, we dissociated the most rostral and inferior part of the anterior cingulate and paracingulate gyri from the median cingulate and medial superior frontal because recent data indicated a cognitive division of these two regions: the rostral part, 30 mm below AC–PC plane (the present definition of the anterior cingulate) being implicated in affective processing (Bush *et al.*, 2000). Finally, the orbital frontal regions were more detailed since the third and fourth frontal sulci were clearly seen on the MNI single-subject brain. As such, the parcellation we propose is very close to that described in the recent work of Chiavaras and Petrides (2000).

The parcellation of the occipital lobe was based on the definition by Dejerine, in which the parietal and occipital gyri show a continuity and where the occipital parcellation of the superior and middle gyri follows that of the parietal lobe. Using this definition, the superior occipital gyrus is in the continuity of the superior parietal gyrus, and the middle occipital gyrus follows the inferior parietal gyrus (Dejerine, 1980). The superior plus the middle occipital regions of the present study correspond to the superior occipital region of Rademacher (Rademacher *et al.*, 1992). The inferior occipital region was limited upward by the inferior occipital sulcus instead of the transverse occipital that has no role in occipital lobe parcellation in the present definition.

We identified three regions in the inferior parietal (supramarginal gyrus, angular gyrus, and some intervening cortex (Salamon *et al.*, 1987)), since in both hemispheres of the MNI single subject, some parts of the inferior parietal lobule belong neither to the supramarginal nor to the angular gyri. The inferior parietal lobule shows a very complex and highly variable cortical pattern and its subdivision is highly dependent from the sulci courses which, from our point of view, does not fit within arbitrary limits.

Labelling of Functional Areas

From the three proposed labeling procedures, the most used in the literature is the simple local maxima labeling. If this method is reliable in single-subject studies, based on the individual brain anatomy, it can lead to some errors in localization in group studies. The limits of all anatomical parcellation are the sulci, which variability has been measured to be 8–10 mm internally and 17–19 mm externally after an affine stereotaxic normalization (Thompson *et al.*, 1996). Thus, a simple local maxima labeling can misplace an activation from one anatomical region to its neighbor as opposed to the use of the extended local maxima labeling approach that seems safer. As shown in the example, a percentage of overlap approximately equal for two regions will point to the fact that either one, or the other, or both, of these regions could be the site of an activation. Following the study by Thompson *et al.* (1996), we choose a 10-mm radius value corresponding to a 20-mm range, the maximal value for variability of external structures. This value is conservative because it takes into account the worst-case scenario, but in the future when quantification of anatomical variability computed from a very large database will become available, this value could be lower for some parts of the brain. Alternately, one can use cluster labeling, but should be aware of its drawbacks since the size of the clusters are dependent on the filter size, which can extend the region in all directions and dramatically increase the false positive level.

SPM interface. Interfacing our parcellation scheme with the SPM package makes this work available to the scientific community with the hope that it will help to standardize the anatomical labeling of PET and functional MRI data. The basic parcellation data structure is simple enough so as to be used in conjunction with other analysis software and other techniques such as MEG and EEG.

ACKNOWLEDGMENT

We are greatly indebted to Dr. Alan Young for reviewing the manuscript.

REFERENCES

Ashburner, J., and Friston, K. J. 1999. Nonlinear spatial normalization using basis functions. *Hum. Brain Mapp.* **7:** 254–266.

Berger, M. S., Cohen, W. A., and Ojemann, G. A. 1990. Correlation of motor cortex brain mapping data with magnetic resonance imaging. *J. Neurosurg.* **72:** 383–387.

Buckner, R. L., Raichle, M. E., Miezin, F. M., and Petersen, S. E. 1996. Functional anatomic studies of memory retrieval for auditory words and visual pictures. *J. Neurosci.* **16:** 6219–6235.

Bush, G., Luu, P., and Posner, M. I. 2000. Cognitive and emotional influences in anterior cingulate cortex. *TICS* **4:** 215–222.

Caviness, V. S., Jr., Meyer, J., Makris, N., and Kennedy, D. N. 1996. MRI-based topographic parcellation of human neocortex: An anatomically specified method with estimate of reliability. *J. Cogn. Neurosci.* **8:** 566–587.

Chi, J. G., Dooling, E. C., and Gilles, F. H. 1977. Gyral development of the human brain. *Ann. Neurol.* **1:** 86–93.

Chiavaras, M. M., and Petrides, M. 2000. Orbitofrontal sulci of the human and macaque monkey brain. *J. Comp. Neurol.* **422:** 35–54.

Collins, D. L., Neelin, P., Peters, T. M., and Evans, A. C. 1994. Automatic 3D intersubject registration of MR volumetric data in standardized Talairach space. *J. Comput. Assist. Tomogr.* **18:** 192–205.

Collins, D. L., Zijdenbos, A., Kollokian, V., Sled, J. G., Kabani, N. J., Holmes, C. J., and Evans, A. C. 1998. Design and construction of a realistic digital brain phantom. *IEEE Trans. Med. Imag.* **17:** 463–468.

Crespo-Facorro, B., Kim, J. J., Andreasen, N. C., O'Leary, D. S., Wiser, A. K., Bailey, J. M., Harris, G., and Magnotta, V. A. 1999. Human frontal cortex: An MRI-based parcellation method. *NeuroImage* **10:** 500–519.

Dejerine, J. 1980. *Anatomie des Centres Nerveux.* Masson, Paris.

Diallo, B., Dolidon, F., Travere, J.-M., and Mazoyer, B. 1998. VoxeLine: A software for 3D real-time visualization of biomedical images. *Comput. Med. Imag. Graph.* **22:** 275–289.

Frank, R. J., Damasio, H., and Grabowski, T. J. 1997. Brainvox: An interactive, multimodal visualization and analysis system for neuroanatomical imaging. *NeuroImage* **5:** 13–30.

Friston, K. J., Ashburner, J., Frith, C. D., Poline, J.-B., Heather, J. D., and Frackowiak, R. S. J. 1995a. Spatial registration and normalization of images. *Hum. Brain Mapp.* **2:** 165–189.

Friston, K. J., Holmes, A. P., Worsley, K. J., Poline, J. B., Frith, C. D., and Frackowiak, R. S. J. 1995b. Statistical parametric maps in functional imaging: A general linear approach. *Hum. Brain Mapp.* **2:** 189–210.

Insausti, R., Juottonen, K., Soininen, H., Insausti, A. M., Partanen, K., Vainio, P., Laakso, M. P., and Pitkanen, A. 1998. MR volumetric analysis of the human entorhinal, perirhinal, and temporopolar cortices. *AJNR* **19:** 659–671.

Kido, D. K., LeMay, M., Levinson, A. W., and Benson, W. E. 1980. Computed tomographic localization of the precentral gyrus. *Radiology* **135:** 373–377.

Kim, J. J., Crespo-Facorro, B., Andreasen, N. C., O'Leary, D. S., Zhang, B. Q., Harris, G., and Magnotta, V. A. 2000. An MRI-based parcellation method for the temporal lobe. *NeuroImage* **11:** 271–288.

Kulynych, J. J., Vladar, K., Jones, D. W., and Weinberger, D. R. 1993. Three-dimentional surface rendering in MRI morphometry: A study of the planum temporale. *J. Comput. Assist. Tomogr.* **17:** 529–535.

Kulynych, J. J., Vladar, K., Jones, D. W., and Weinberger, D. R. 1994. Gender differences in the normal lateralization of the supratemporal cortex: MRI surface-rendering morphometry of Heschl's gyrus and the planum temporale. *Cereb. Cortex* **4:** 107–118.

Lancaster, J. L., Woldorff, M. G., Parsons, L. M., Liotti, M., Freitas, C. S., Rainey, L., Kochunov, P. V., Nickerson, D., Mikiten, S. A., and Fox, P. T. 2000. Automated Talairach atlas labels for functional brain mapping. *Hum. Brain Mapp.* **10:** 120–131.

Maddock, R. J. 1999. The retrosplenial cortex and emotion: New insights from functional neuroimaging of the human brain. *TINS* **22:** 310–316.

Mai, J. K., Assheuer, J., and Paxinos, G. 1997. *Atlas of the Human Brain.* Academic Press, San Diego.

Ono, M., Kubik, S., and Abernathey, C. D. 1990. *Atlas of the Cerebral Sulci.* Thieme, New York.

Paus, T., Tomaiuolo, F., Otaky, N., MacDonald, D., Petrides, M., Atlas, J., Morris, R., and Evans, A. C. 1996. Human cingulate and

paracingulate sulci: Pattern, variability, asymmetry, and probabilistic map. *Cereb. Cortex* **6:** 207–214.

Penhune, V. B., Zatorre, R. J., MacDonald, J. D., and Evans, A. C. 1996. Interhemispheric anatomical differences in human primary auditory cortex: Probabilistic mapping and volume measurement from magnetic resonance scans. *Cereb. Cortex* **6:** 661–672.

Petit, L., Courtney, S., Ungerleider, L. G., and Haxby, J. V. 1998. Sustained activity in the medial wall during working memory delays. *J. Neurosci.* **18:** 9429–9437.

Quinton, O., Vérard, L., Tzourio, N., Bloyet, D., and Travère, J. M. 1997. Automatic AC-PC identification on 3D T1-MRI using scene analysis. *NeuroImage* **5:** S405.

Rademacher, J., Caviness, V. S., Steinmetz, H., and Galaburda, A. M. 1993. Topographical variation of the human primary cortices: implications for neuroimaging, brain mapping, and neurobiology. *Cereb. Cortex* **3:** 313–329.

Rademacher, J., Galaburda, A. M., Kennedy, D. N., Filipek, P. A., and Caviness, V. S. 1992. Human cerebral cortex: Localization, parcellation, and morphometry with magnetic resonance imaging. *J. Cogn. Neurosci.* **4:** 352–374.

Rajkowska, G., and Goldman-Rakic, P. S. 1995. Cytoarchitectonic definition of prefrontal areas in the normal human cortex. II. Varaibility in the locations of areas 9 and 46 and relationship to the Talairach coordinates system. *Cereb. Cortex* **5:** 323–337.

Rumeau, C., Tzourio, N., Murayama, N., Peretti-Vitton, P., Levrier, O., Joliot, M., Mazoyer, B., and Salamon, G. 1994. Location of hand function in the sensorimotor cortex: Magnetic resonance and functional correlation. *AJNR* **15:** 562–572.

Salamon, G., Gelbert, F., Alicherif, A., Poncet, M., Khalil, R., Sobel, D., Von Einseidel, O., Morel, M., and Corbaz, J. M. 1987. Le repérage *in vivo* des aires du langage. *Rev. Neurol.* **143:** 580–587.

Sastre-Janer, F., Regis, J., Belin, P., Mangin, J.-F., Dormont, D., Masure, M. C., Remy, P., Frouin, V., and Samson, Y. 1998. Three dimensional reconstruction of the human central sulcus reveals a morphological correlates of the hand area. *Cereb. Cortex* **8:** 641–647.

Schleicher, A., Amunts, K., Geyer, S., Morosan, P., and Zilles, K. 1999. Observer-independent method for microstructural parcellation of cerebral cortex: A quantitative approach to cytoarchitectonics. *NeuroImage* **9:** 165–177.

Schmahmann, J. D., Doyon, J., McDonald, D., Holmes, C., Lavoie, K., Hurwitz, A. S., Kabani, N., Toga, A., Evans, A., and Petrides, M. 1999. Three-dimensional MRI atlas of the human cerebellum in proportional stereotaxic space. *NeuroImage* **10:** 233–260.

Shapleske, J., Rossell, S. L., Woodruff, P. W., and David, A. S. 1999. The planum temporale: A systematic, quantitative review of its structural, functional and clinical significance. *Brain Res. Rev.* **29:** 26–49.

Sled, J. G., Zijdenbos, A., and Evans, A. C. 1998. A non-parametric method for automatic correction of intensity non-uniformity in MRI data. *IEEE Trans. Med. Imag.* **17:** 87–97.

Sobel, D. F., Gallen, C. C., Schwartz, B. J., Waltz, T. A., Copeland, B., Yamada, S., Hirschkoff, E. C., and Bloom, F. E. 1993. Locating the central sulcus: Comparison of MR anatomic and magnetoencephalographic functional methods. *AJNR* **14:** 915–925.

Steinmetz, H., Fürst, G., and Freund, H.-J. 1990. Variation of perisylvian and calcarine anatomical landmarks within stereotaxic proportional coordinates. *AJNR* **11:** 1123–1130.

Talairach, J., and Tournoux, P. 1988. *Co-planar Stereotaxic Atlas of the Human Brain 3-Dimensional Proportional System: An Approach to Cerebral Imaging.* Stuttgart, New York.

Thompson, P. M., Schwartz, C., Lin, R. T., Khan, A. A., and Toga, A. W. 1996. Three-dimensional statistical analysis of sulcal variability in the human brain. *J. Neurosci.* **16:** 4261–4274.

Tzourio, N., Petit, L., Mellet, E., Orssaud, C., Crivello, F., Benali, K., Salamon, G., and Mazoyer, B. 1997. Use of anatomical parcellation to catalog and study structure function relationships in the human brain. *Hum. Brain Mapp.* **5:** 228–232.

Westbury, C. F., Zatorre, R. J., and Evans, A. C. 1999. Quantifying variability in the planum temporale: A probability map. *Cereb. Cortex* **9:** 392–405.